Chapter 3
Mediastinal Masses: Radiological Point of View

Alfonso Reginelli, Anna Russo, Fernando Scala, Elisa Micheletti, Roberta Grassi, Mario Santini, and S. Cappabianca

Introduction

Mediastinal masses are relatively uncommon [1]. Because such a wide variety of other pathologic entities can occur in this region, radiologists and clinicians will encounter many of these specific lesions only infrequently. Imaging is a critical part of establishing a presumptive diagnosis, which is used to guide whether and what type of confirmatory testing is needed. When classic features are present, a presumptive diagnosis can be made with a high degree of confidence based on imaging alone. Developing an appropriate differential diagnosis for a particular patient can be very useful in avoiding unnecessary and sometimes misleading biopsies or additional tests. The mediastinum contains vital vascular and nonvascular structures and organs [2, 3]. In many instances, localization and characterization of a mediastinal abnormality using multidetector CT are enough to make a diagnosis. In other cases, correlation between imaging findings and clinical context, as well as additional

A. Reginelli (✉) · A. Russo · F. Scala · E. Micheletti · S. Cappabianca
Radiology and Radiotherapy Unit, Department of Clinical and Experimental Medicine, Università degli Studi della Campania "Luigi Vanvitelli", Naples, Italy
e-mail: alfonso.reginelli@unicampania.it; annarusso81@yahoo.itl; scala.fernando@gmail.com; elisamic88@alice.it; salvatore.cappabianca@unicampania.it

R. Grassi
Radiotherapy Unit, Department of Biomedical, Experimental and Clinical Sciences "Mario Serio", University of Florence, Florence, Italy
e-mail: roberto.grassi@unina2.it

M. Santini
Thoracic Surgery Unit, Department of Translational Medical Science, Università degli Studi della Campania 'Luigi Vanvitelli', Naples, Italy
e-mail: mario.santini@unicampania.it

R. Franco et al. (eds.), *The Mediastinal Mass*, Current Clinical Pathology,
https://doi.org/10.1007/978-3-319-90368-2_3

imaging examinations (such as MR imaging and fluorodeoxyglucose (FDG) positron emission tomography (PET)/CT and histologic sampling through image guided or surgical biopsy), is necessary to make a definitive diagnosis and guide further management. Employing the existing nomenclature of the mediastinal compartments, slightly more than half of all mediastinal masses are located in the anterior compartment, whereas one fourth are identified in the middle and posterior mediastinal compartments. Division of the mediastinum into specific compartments has traditionally been valuable in the identification, characterization, and management of various mediastinal abnormalities [4].

The existing schemes used in radiologic practice represent arbitrary non-anatomic divisions of the chest, primarily based on the lateral chest radiograph. Division of the mediastinum into specific compartments is favorable for a number of reasons, including the generation of a focused differential diagnosis, assistance in planning for biopsies and surgical procedures, and the facilitation of communication between clinicians in a multidisciplinary setting. Several classification schemes for the mediastinum have been created and used. Most radiologic classifications have been based on arbitrary landmarks outlined on the lateral chest radiograph. A new scheme, based on cross-sectional imaging (principally multidetector computed tomography), has been developed by the International Thymic Malignancy Interest Group (ITMIG) and accepted as the new standard. This clinical division scheme defines unique prevascular, visceral, and paravertebral compartments based on boundaries delineated by specific anatomic structures at multidetector CT [4]. This new definition plays an important role in the identification and characterization of mediastinal abnormalities, which can often be diagnosed with confidence, based on their location and imaging features alone. In other cases, a diagnosis maybe suggested when radiologic features are combined with specific clinical information. This new definition plays an important role in the identification and characterization of mediastinal abnormalities, which, although uncommon and encompassing a wide variety of entities, can often be diagnosed with confidence based on location and imaging features alone. The three compartment cross-sectional imaging model developed by ITMIG includes prevascular (anterior), visceral (middle), and paravertebral (posterior) sections. Specific compartment boundaries and the anatomic structures contained can be readily identified at multidetector CT.

Radiological Anatomy

Prevascular Compartment

The following boundaries of the prevascular compartment are defined as (a) superiorly, the thoracic inlet; (b) inferiorly, the diaphragm; (c) anteriorly, the posterior border/cortex of the sternum; (d) laterally, the parietal mediastinal pleura; and (e) posteriorly, the anterior aspect of the pericardium as it wraps around the heart in a curvilinear shape. The major contents of the prevascular compartment include the thymus, fat, lymph nodes, and the left brachiocephalic vein [5–10]. Therefore, the

most common abnormalities encountered in the prevascular compartment include thymic lesions (cysts, hyperplasia, and malignancies such as thymomas, thymic carcinomas, and neuroendocrine neoplasms), germ cell neoplasms (which derive from germ cell rest remnants in the mediastinum), lymphomas, metastatic lymphadenopathies, and intrathoracic goiters.

Visceral Compartment

The following boundaries of the visceral compartment are defined: (a) superiorly, the thoracic inlet; (b) inferiorly, the diaphragm; (c) anteriorly, the posterior boundaries of the prevascular compartment; and (d) posteriorly, a vertical line connecting a point on the thoracic vertebral bodies 1 cm posterior to the anterior margin of the spine (referred to as the visceral paravertebral compartment boundary line). The major contents of the visceral compartment can be divided into two main categories: (a) vascular structures including the heart, superior vena cava, ascending thoracic aorta, aortic arch, descending thoracic aorta, intrapericardial pulmonary arteries, and thoracic duct and (b) nonvascular structures including the trachea, carina, esophagus, and lymph nodes. The most common abnormalities in the visceral compartment include lymphadenopathies (related to lymphomas or metastatic disease), duplication cysts, tracheal lesions, and esophageal neoplasms. Additionally, vascular lesions deriving from the heart, pericardium, and great vessels may also be present.

Paravertebral Compartment

The following boundaries of the paravertebral compartment are defined: (a) superiorly, the thoracic inlet; (b) inferiorly, the diaphragm; (c) anteriorly, the posterior boundaries of the visceral compartment; and (d) posterolaterally, a vertical line along the posterior margin of the chest wall at the lateral side of the transverse processes. The major contents of the paravertebral compartment include the thoracic spine and paravertebral soft tissues; therefore, most abnormalities in this region are neurogenic neoplasms that arise from the dorsal root ganglia/neurons adjacent to the intervertebral foramina [8–11]. Other potential lesions in this compartment may have infective (discitis/osteomyelitis) or traumatic (hematoma) origin or may be related to other underlying conditions (such as extramedullary hematopoiesis). Although localization of mediastinal lesions in a specific compartment is an important component of characterization, this may be difficult in some instances as in the case of large mediastinal lesions that may involve multiple compartments or extend from one compartment to another, making identification of the precise site of origin challenging, for example. Two tools have been described by ITMIG and are recommended to help identify the compartments of origin. One of these tools is known as the “center method” and states that the center of a mediastinal lesion (defined as the

center point of the lesion on the axial CT image that demonstrates the largest size of the abnormality) localizes the lesion to a specific mediastinal compartment [11, 12]. The JART study used this method, and the result was an accurate localization of all 445 mediastinal masses. The second tool is known as the "structure displacement tool" and is useful in scenarios in which very large mediastinal lesions displace organs from other mediastinal compartments, typically those that abut the compartment from which the lesion originated [12]. For instance, a very large prevascular mediastinal mass may displace organs of the visceral mediastinal compartment, such as the trachea, esophagus, or the heart posteriorly.

Role of Diagnostic Imaging

ITMIG uses multidetector CT as the gold standard modality for defining the mediastinal compartments. Specific imaging characteristics that should be noted at multidetector CT include (a) location, size, and configuration of mediastinal lesions; (b) descriptive features such as attenuation, heterogeneity, and enhancement; (c) presence of intralesional fat, cystic components, soft tissue, and calcification; and (d) any connection or invasion of adjacent structures. Some of these findings are more important than others; for instance, the presence of fat in a prevascular mediastinal lesion is highly suggestive of a smaller group of specific diseases, whereas punctate, coarse, or curvilinear calcifications are nonspecific and can't be used to discriminate benign from malignant prevascular mediastinal masses, because they may be associated with malignant neoplasms such as thymomas or treated lymphomas, as well as benign lesions such as mature teratomas [13, 14].

It is important to consider findings suggestive of a mediastinal abnormality at chest radiography, as it remains the most common imaging examination performed. Although small lesions may not be visible or may produce only subtle findings, large mediastinal abnormalities may manifest in a variety of ways, such as a soft-tissue masses, often accompanied by loss of the normal mediastinal contours or interfaces or thickening of specific lines or stripes. The lateral chest radiograph can be especially useful in detecting lesions that may not be visible on the posteroanterior radiograph, since mediastinal lesions may be only visible in the retrosternal space or when overlying the upper thoracic spine.

The "silhouette sign," which describes the loss of normal borders of intrathoracic structures, aids in the detection of mediastinal abnormalities. A lesion in the right aspect of the anterior mediastinum may obscure cardiovascular structures, such as the superior vena cava or right heart border. While a mass in the posterior mediastinum may result in the loss of the normal paraspinal stripes. The "hilum overlay" sign may help differentiate a mediastinal mass from cardiomegaly or enlarged pulmonary vessels.

The "cervicothoracic sign," described by Felson [8], is useful in localizing mediastinal abnormalities identified at radiography and making a focused differential diagnosis. In these cases, obscuration of the lateral borders of an upper mediastinal

mass as it extends above the clavicles into the neck implies that the lesion has both intrathoracic and cervical components. Although often misinterpreted as a manifestation of the cervicothoracic sign, an upper paravertebral (or posterior mediastinal) mass with visible edges above the clavicles is entirely located within the chest, but does not exhibit the cervicothoracic sign.

While MR imaging is not the first used exam for the evaluation of all mediastinal abnormalities, it is the most useful imaging modality to distinguish cystic from solid lesions (e.g., thymic cysts from solid neoplasms), discern cystic and/or necrotic components within solid masses, distinguish cystic neoplasms from benign cysts, and identify septa and/or soft tissue within cystic lesions. The role of fluorine-18-FDG PET/CT in the evaluation of many mediastinal abnormalities remains controversial. It has been observed that thymic epithelial neoplasms tend to demonstrate variable, often only low-grade FDG uptake, making the histologic differentiation between the various types of neoplasms unreliable. A significant factor limiting the ability of PET/CT to accurately characterize mediastinal lesions is the potential for false-positive and false-negative examinations. Some benign processes, such as thymic hyperplasia and inflammatory diseases (such as fibrosing mediastinitis), may demonstrate increased FDG uptake and mimic malignancy. In these cases, a combination of clinical history, focality of FDG uptake at PET/CT, and morphologic features at multidetector CT is necessary to determine whether the lesion is benign or malignant [15–19].

Masses of Prevascular Compartment

The true incidence of prevascular mediastinal masses is difficult to detect for multiple reasons: the most significant one is the use of different classification schemes [20]. Additionally, there is variability in the inclusion of nonneoplastic lesions such as thymic hyperplasia, thymic and pericardial cysts, and other neoplastic lesions such as lymphomas [20]. The most common neoplasms of the prevascular mediastinum include thymic epithelial neoplasms (thymomas, thymic carcinomas, and thymic neuroendocrine tumors) and lymphomas. Other neoplasms that may arise in the prevascular compartment include mature teratomas, nonteratomatous germ cell malignancies (such as seminomas), nonseminomatous germ cell neoplasms, and metastatic disease. Nonneoplastic lesions of the prevascular mediastinum include substernal extensions of thyroid goiters, thymic hyperplasia, cystic lesions such as thymic and pericardial cysts, and vascular lymphatic abnormalities [21–25].

Thyroid Goiter: A heterogeneous prevascular mediastinal mass that demonstrates continuity with the cervical thyroid gland, intrinsically hyperattenuates (HU 70–85 due to the presence of iodine), and shows a sustained and intense enhancement after administration of intravenous contrast material, can dependably be diagnosed as a mediastinal goiter. Cystic changes which manifest as internal foci of low attenuation and calcifications may also be present. In cases where a definitive connection with the cervical thyroid gland cannot be identified, the use of multidetector CT

should strongly suggest the diagnosis. When additional findings, such as the loss of mediastinal tissue planes or associated cervical or mediastinal lymphadenopathy, accompany a mediastinal goiter, then thyroid malignancy should be suspected, and further evaluation should be performed [26, 27] (Figs. 3.1 and 3.2).

Fat-containing Lesions: The presence of visible regions of intralesional fat (measuring between −40 and −120 HU at multidetector CT) within a heterogeneous prevascular mediastinal mass is highly suggestive of a mature teratoma. Patients may have symptoms related to local mass effect or be asymptomatic (Figs. 3.3 and 3.4). Moreover, associations between thymolipoma and myasthenia gravis have been reported. Graves' disease and hematologic disorders have also been reported [26, 27].

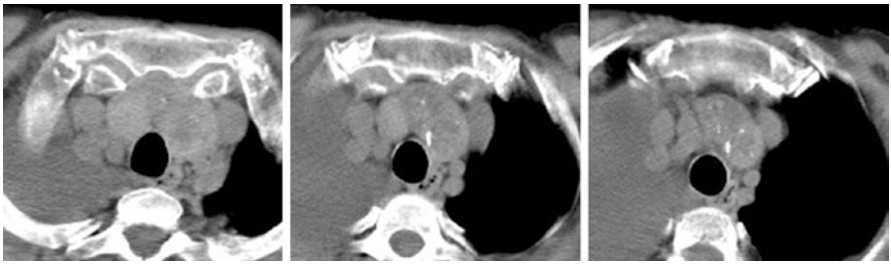

Fig. 3.1 Chest CT without contrast. Immersed thyroid goiter. Hypodense nodules with contextual calcifications

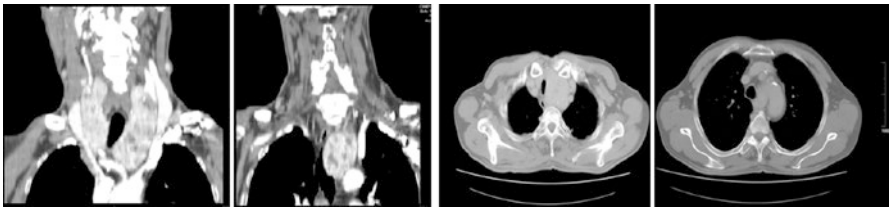

Fig. 3.2 Neck and chest CT with and without contrast: cervico-mediastinal goiter. It is observed inhomogeneous and enlarged thyroid gland that takes advantage in the mediastinum with lateral deviation of the trachea to the right which is partly compressed

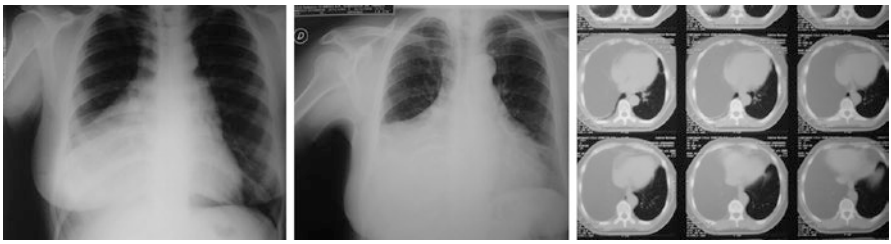

Fig. 3.3 Chest X-ray/chest CT without contrast: lipomatosis. In X-ray, presence of x-opacity in the right basal hemithorax with obliteration of the homolateral costophrenic sinus. At CT, non-ca

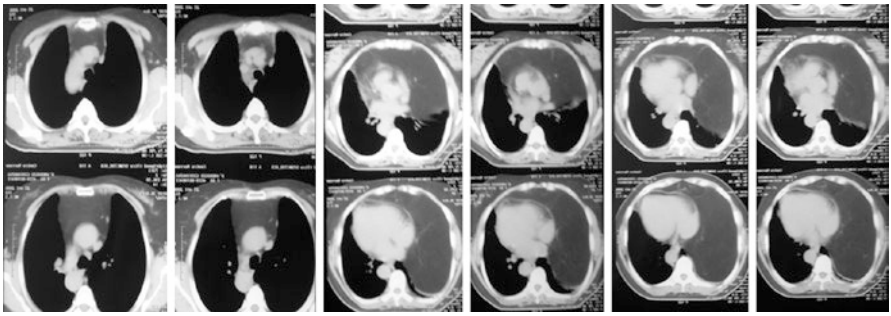

Fig. 3.4 Chest CT without contrast: lipomatosis. Increase of non-capsulated adipose tissue in the anterior mediastinum extending in left hemithorax and with contralateral dislocation of medial structures

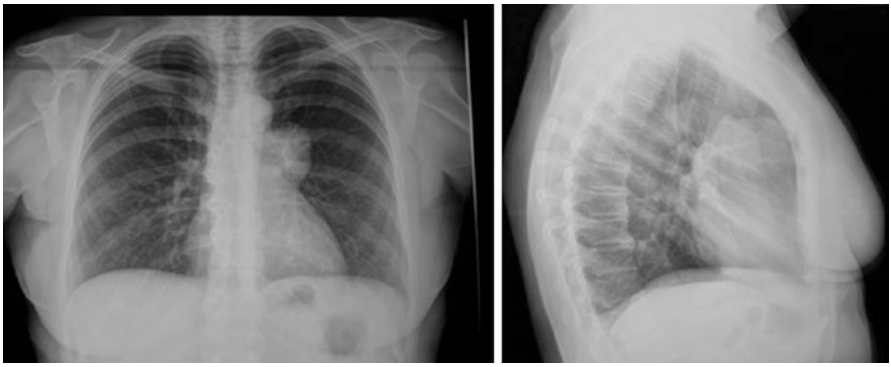

Fig. 3.5 Chest X-ray: thymic cyst. Radiopaque nodular formation is observed at the level of the II aortic arch

Cystic Lesions: Cystic lesions of the mediastinum are those that have water or fluid attenuation at multidetector CT, with Hounsfield unit values between 0 and 20. A well-circumscribed homogeneous lesion in the prevascular mediastinum, near the thymic bed that is rounded, oval, or saccular, likely represents a thymic cyst (Fig. 3.5). Most of these lesions are acquired and caused by inflammation; iatrogenic processes such as surgery, radiation therapy, or chemotherapy; or malignant neoplasms. Prevascular masses that are purely cystic with no soft-tissue components or internal septa can reliably be diagnosed as unilocular thymic cysts [28]. However, when cystic lesions contain internal soft-tissue components and/or internal septa, the differential diagnosis should include multilocular thymic cysts, cystic teratomas, lymphangiomas, and cystic thymomas.

Thymic Hyperplasia: Normal prevascular thymic tissue is seen in young individuals and decreases in prominence with advancing age, with complete fatty replacement, usually achieved by 40 years of age. Two distinct histologic types of thymic hyperplasia have been described: true and thymic lymphoid (follicular)

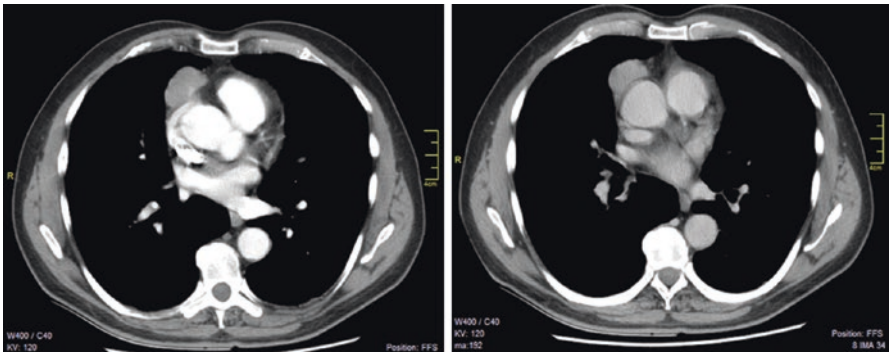

Fig. 3.6 Chest CT with contrast: infiltrating thymoma. Presence of hypodense tissue that seems to infiltrate the pericardium

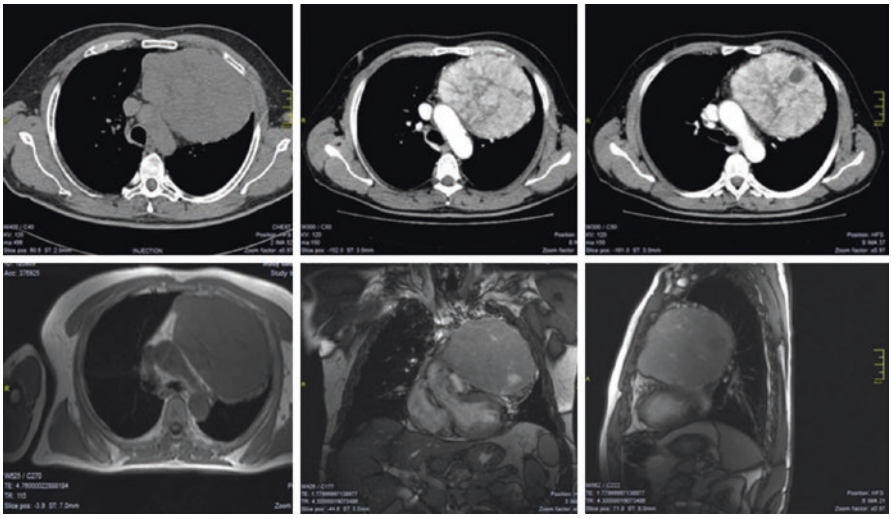

Fig. 3.7 Chest CT scan without and with mdc/chest MRI with T1w and T2w sequences: thymoma. Voluminous and inhomogeneous mass, occupying space: hypodense in sequences without contrast and it becomes hyperdense after contrast medium. At the MRI, it appears hypointense in both T1w and T2w sequences with some hyperintense spots in the T2w sequences to refer to probable colliquation phenomena

hyperplasia. True thymic hyperplasia is also known (Figs. 3.6 and 3.7) as "rebound hyperplasia" and is characterized by an increase in thymic volume that becomes greater than 50% over baseline after a causative stressor; approximately 10–25% of patients undergoing chemotherapy may develop rebound hyperplasia [29]. Thymic lymphoid (follicular) hyperplasia is a histologic diagnosis defined as the presence of an increased number of lymphoid follicles, which may be associated with an increase in the size of the gland and is typically associated with immunologic

diseases, such as myasthenia gravis, hyperthyroidism, collagen vascular diseases, or human immunodeficiency virus infection [10].

Lymphomas: A mildly enhancing lobular soft-tissue mass or group of enlarged lymph nodes in the prevascular mediastinum at multidetector CT, especially in the setting of lymphadenopathy in the neck, axilla, or elsewhere in the body, may represent a lymphoma (Figs. 3.8, 3.9, 3.10, and 3.11). Although it may be difficult to distinguish lymphomas from other soft-tissue mediastinal masses, the infiltrative nature of some types of lymphomas enables differentiation from thymic epithelial neoplasms and germ cell tumors.

Nonteratomatous Germ Cell Neoplasms: Nonteratomatous germ cell neoplasms include a wide variety of lesions, the most common of which include seminomatous and nonseminomatous germ cell tumors (NSGCTs). These lesions typically manifest as large soft-tissue masses in the prevascular mediastinum and can be difficult to distinguish from lymphomas.

Ectopic Parathyroid Adenomas: In patients with a clinical history of primary hyperparathyroidism, elevated serum calcium levels, and/or elevated serum

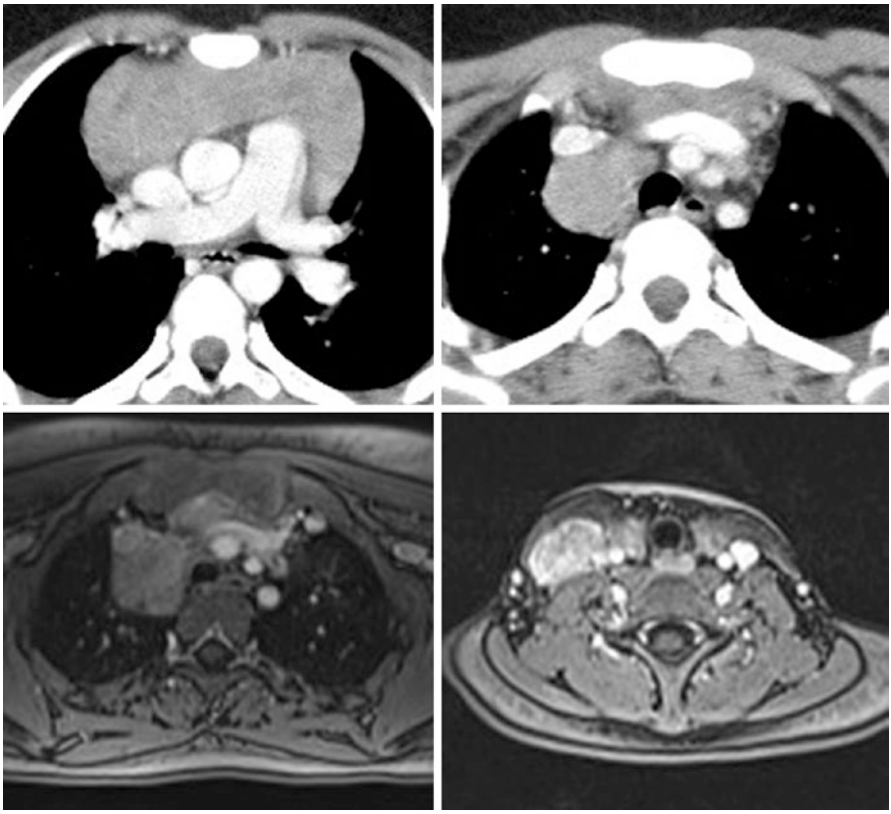

Fig. 3.8 Chest and neck CT/MRI with contrast. Recurrence of mediastinal lymphoma with involvement of the supraclavicular region

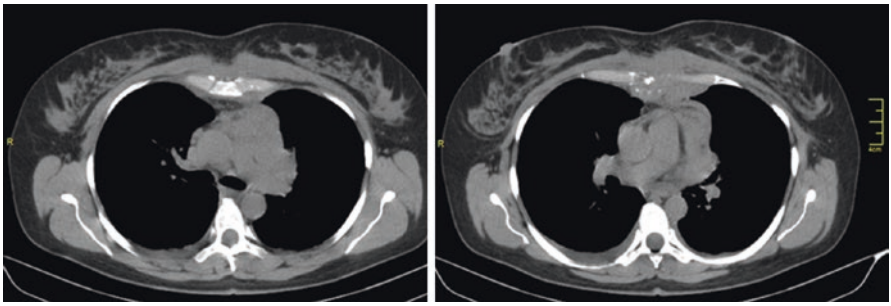

Fig. 3.9 Chest CT without contrast: Hodgkin's lymphoma infiltrating the breastbone

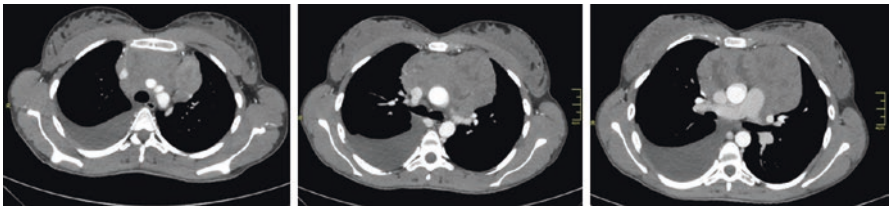

Fig. 3.10 Chest CT with contrast: non-Hodgkin lymphoma B cells of the thymus. There is an inhomogeneous, partly colliquated mass located in the anterior mediastinum. AR: right pleural effusion is observed

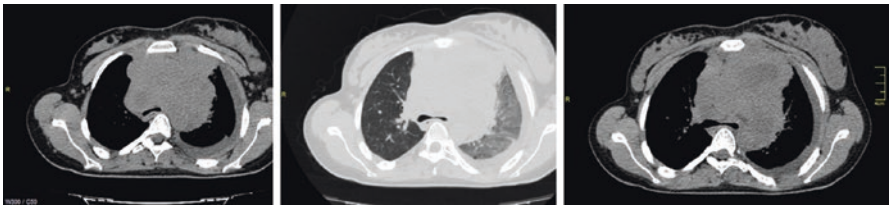

Fig. 3.11 Chest CT without contrast: non-Hodgkin lymphoma B-cell. It is observed hypodense and inhomogeneous mass occupying the mediastinum

parathyroid hormone levels, a soft-tissue nodule in the prevascular mediastinum at multidetector CT should be suspected as ectopic parathyroid adenoma. Although most parathyroid adenomas are juxtathyroid in location, they may occur in an ectopic location, with the mediastinum being the most common such site [30]. Many different imaging modalities can assist in the diagnosis of these lesions, including high-resolution ultrasonography (US) with color Doppler, technetium-99m (99mTc) sestamibi single photon emission CT (SPECT), multidetector CT, and MR imaging.

Morgagni Hernias: The major entity in the differential diagnosis of a thymolipoma is a Morgagni hernia. These hernias contain omental fat that has herniated from the abdomen into the thorax via the foramen of Morgagni [31]; the fat locates in a retrosternal or parasternal location, usually on the right side. Occasionally,

Morgagni hernias can also contain small or large bowel or portions of the liver. On CT, a Morgagni hernia appears as a fat-containing mass in the lower, anterior mediastinum that is usually large in size.

Masses of Visceral Compartment

The most common abnormalities in the visceral compartment include lymphadenopathy (related to lymphoma or metastatic disease), duplication cysts, tracheal lesions, and esophageal neoplasms. Additionally, vascular lesions arising from the heart, pericardium, and great vessels may also be present.

Cystic Lesions: A well-circumscribed, homogeneous, fluid attenuation lesion measuring 0–20 HU at multidetector CT in the visceral mediastinal compartment is compatible with benign duplication cysts, the most common of which include bronchogenic and esophageal duplication cysts. At multidetector CT, bronchogenic cysts manifest as a single, smooth, round, or ovoid masses with internal low attenuation (Fig. 3.12). The wall has variable perceptibility and may enhance or demonstrate intrinsic calcifications. Esophageal duplication cysts are uncommon developmental anomalies that manifest as well-circumscribed, homogeneous, fluid attenuation lesions adjacent to the esophagus or associated with the esophageal wall at multidetector CT. On CXR, esophageal cysts appear as solitary, rounded, well-defined mediastinal lesions, similar to other foregut cysts [8]. On CT they appear as single homogeneous masses with regular and well-defined borders and low-to-high attenuation values, due to their fluid or proteinaceous content, respectively [25, 26]. They are located in the lower right part of the posterior mediastinum within the esophageal wall or closely adjacent to it [3]. A thick wall and calcification may help in distinguishing an esophageal duplication cyst from other foregut cysts [3, 25]. On MRI, esophageal duplication cysts have high signal intensity on T2-weighted images and are usually of low signal intensity on T1-weighted sequences [12]. Contrast administration is recommended on both CT and MRI, as the complete absence of enhancement within the cyst is characteristic of benignity [25]. 99mTechnetium-pertechnetate scans can help in the identification of esophageal cysts containing ectopic gastric mucosa, which are at higher risk of developing cyst rupture and hemorrhage [32, 33].

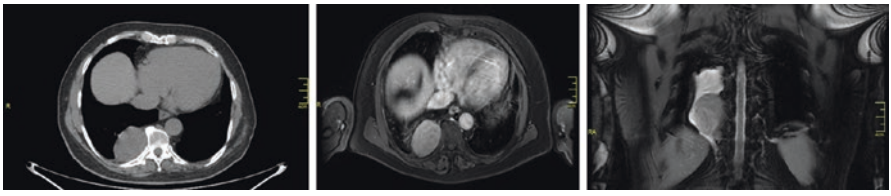

Fig. 3.12 Chest MRI T2w sequence/chest TC without contrast: neuroma type A. In CT hypodense nodular formation in right paravertebral site and hypointense in MRI

Esophageal Varices: These typically occur in the distal esophagus as a result of portal hypertension ("uphill varices") and bleed in a third of cases, representing a life-threatening complication in cirrhotic patients [34]. Less commonly they can be caused by superior vena cava obstruction ("downhill varices") and are usually located in the upper esophagus [35]. The reference standard for the diagnosis of esophageal varices is upper gastrointestinal endoscopy [36]. However, CT is a valuable tool for evaluating the cirrhotic liver and generally provides adequate coverage of the distal esophagus, where almost all varices develop.

Esophageal Neoplasms: These can be malignant (80%) or benign (20%). Malignant esophageal neoplasms are mainly squamous cell carcinomas and adenocarcinomas [37]. Once the histologic diagnosis is confirmed, CT of the chest and abdomen is recommended to assess local and distant spread of disease [37]. Oral and intravenous contrast material should be used to improve visualization of the esophageal lumen and mediastinal structures [38]. MRI does not substantially improve nodal staging, and its overall diagnostic performance does not exceed the abovementioned techniques [34, 39]. Malignant esophageal tumors usually produce intermediate signal intensity on T2-weighted images, unless they contain a high amount of extracellular mucin, which characteristically causes them to become hyperintense on these sequences.18F-FDG-PET scanning is recommended to improve the accuracy of staging of distant disease in patients who are potential candidates for curative therapy, whereas the value of 18F-FDG-PET as a predictive marker of response to neoadjuvant therapy remains uncertain [40].

Cardiac Masses: When a mass involving the heart or pericardium is identified at multidetector CT, a wide variety of malignant and benign lesions should be considered. One of the most important features is the location of the abnormality, as masses can be categorized as intracavitary, valvular, intramural, or epicardial/pericardial. Other significant features include composition (soft tissue, fat, calcium, and attenuation), behavior (well-defined or infiltrative), and enhancement characteristics after administration of intravenous contrast material.

Thoracic Aortic Aneurysms: An aortic aneurysm is defined as a permanent localized dilatation of the aorta, having at least a 50% increase in the expected normal diameter [41]. Rupture of a descending aortic aneurysm usually occurs in the mediastinum and the left pleural space, producing a periaortic soft-tissue hematoma, hemothorax, pleural or pericardial effusion, or even a contrast blush of active extravasation at the site of rupture [42]. Dissection is the most common aortic emergency and has a poor prognosis. It results from a tear in the intimal layer of aortic wall, allowing inflow of blood through the medial layer. This creates a "false lumen" that is separated from the "true lumen" by an intimal flap. According to the Stanford classification, dissections of the ascending aorta are categorized as type A and account for 62% of cases, whereas dissections of the descending aorta are categorized as type B and account for 38% of cases [43]. Type A dissections require urgent surgical repair, as they have a mortality rate over 50% within 48 h if untreated [44]. Conversely, type B dissections are generally managed conservatively, with follow-up examinations every 3–6 months [36]. Contrast-enhanced CT rapidly determines the type of dissection. It demonstrates the intimal flap in 70% of cases, the entry and

reentry points, signs of rupture, alterations of organ perfusion, dilation of the false lumen, and extension of the process into the aortic valve [43].

Masses of Paravertebral Compartment

As the paravertebral compartment includes the thoracic spine and paravertebral soft tissues, most lesions originating in this region are neoplasms of neurogenic origin. Other less common neoplastic conditions in this compartment include lymphomas, primary osseous tumors, and metastases. Nonneoplastic causes include thoracic spinal infections due to bacterial and mycobacterial agents, cystic lesions such as thoracic meningoceles and neurenteric cysts, and extramedullary hematopoiesis.

Neurogenic Tumors: Up to 95% of neurogenic tumors occur in the posterior mediastinum and are the most common posterior mediastinal masses [2, 3]. According to the cell of origin, neurogenic tumors are divided into three groups: nerve sheath tumors, sympathetic ganglion cell tumors, and paraganglionic cell tumors. Nerve sheath tumors are the most common type of neurogenic tumors in adults [45]. They include benign schwannomas and neurofibromas, as well as malignant peripheral nerve sheath tumors. Sympathetic ganglion tumors, the most common type in children [3, 4], have various histologic grades of aggressiveness. Ganglioneuromas are considered benign, despite their potential to metastasize. Ganglioneuroblastomas have intermediate aggressiveness, and neuroblastomas are the most aggressive form. Paraganglionic cell tumors in the posterior mediastinum are rare and arise along the sympathetic chain, in the so-called aortosympathetic paraganglia [46]. On CXR, the smoothly rounded or oval opacities caused by neurogenic tumors obliterate the paraspinal lines and can be associated with scalloping of the adjacent bones [5]. On CT, the sharply defined soft-tissue masses in the paravertebral area have a variable appearance, ranging from an iso- or hypoattenuating mass to heterogeneous lesions containing hemorrhage, necrosis, cystic degeneration, calcifications, and areas of patchy fat [45]. CT is superior to CXR in demonstrating erosion or scalloping of adjacent ribs and vertebral bodies. In tumors extending through the intervertebral foramina, CT also shows the typical "dumbbell" appearance. After contrast injection, small paragangliomas show avid and homogeneous enhancement, whereas ganglioneuromas show subtle enhancement in the arterial phase and mild enhancement in the delayed phase [46]. No typical enhancement characteristics have been reported for other types of neurogenic tumors. Rapid growth, necrosis, and hemorrhage are CT findings suggestive of malignancy. Finally, CT is the imaging modality used for assessing distant metastases to the bones, lungs, and liver, which are common sites of metastasis for neuroblastomas. MRI helps to differentiate between individual neurogenic tumors. Paragangliomas show a characteristic "salt-and-pepper" appearance on T1-weighted images, due to the presence of multiple curvilinear and punctate signal voids that correspond to high-velocity flow in intratumoral vessels [9]. Conversely, on T2-weighted images, ganglioneuromas may present a "whorled" appearance [6,

10], while neurofibromas may show a "target" pattern, defined as a central portion with lower signal intensity than the peripheral zone. MRI accurately demonstrates the presence and extent of intraspinal tumors, invasion of adjacent neural structures, and encasement of vessels, which all influence surgical treatment and management. Metaiodobenzylguanidine scintigraphy is highly sensitive for determining the extent of disease in catecholamine-producing neuroblastomas and paragangliomas. 18F-fluorodeoxyglucose positron emission tomography (18F-FDG-PET) scanning has reasonable accuracy (82%) in distinguishing malignant forms from benign forms.

Infectious Spondylitis: Infectious spondylitis is usually caused by pyogenic or tuberculous infections with the latter being known as Pott's disease [47]. Hematogenous spread is the most common pathway of infectious spondylitis, but direct inoculation, contiguous extension, or lymphatic drainage from adjacent affected areas may also occur. Infection of a vertebral body may extend into the prevertebral and paravertebral soft tissues, spreading via the anterior or posterior longitudinal ligaments [48, 49]. Early stages of paravertebral abscesses and bone destruction may be difficult to detect on CXR. Conversely, CT and MRI have a high sensitivity for detecting early osteolytic destruction of the vertebrae, accompanying focal or diffuse paraspinal soft-tissue abscesses, intervertebral disc involvement, and epidural granulation tissue [48]. Osteolytic destruction of the vertebrae may cause collapse, more commonly in the anterior part, leading to the characteristic gibbus deformity in Pott's disease. Paravertebral soft-tissue abscesses typically appear as a "horseshoe" mass surrounding an affected vertebral body. They may extend over several vertebral segments above and below the site of bone destruction. On CT, theses abscesses have soft-tissue density. On MRI, they have decreased signal intensity on T1-weighted images and increased signal intensity on T2-weighted images [48]. Contrast material improves the detection of paraspinal abscesses on both CT and MRI. Pyogenic abscess usually has a thick and irregular enhancement wall, in contrast to the thin and smooth enhancement of the wall of tuberculous abscesses. Other helpful features in the differential diagnosis between tuberculous and pyogenic abscesses include calcifications in tuberculous infections and hypodensities or complete destruction of the intervertebral disc in pyogenic infections, which are best visualized on CT [49]. In addition, MRI allows for the assessment of epidural masses with nerve root or spinal cord compression. More than 80% of patients with extramedullary hematopoiesis are asymptomatic, with the condition being incidentally detected at imaging [48]. Rarely, there may also be pleural effusions, hemothoraces, or respiratory failure. Cord compression can cause back pain, lower extremity weakness, numbness, and even paraplegia. CXR shows smooth, well-delineated paraspinal masses, which may be associated with trabeculated and widened ribs in patients with chronic anemia. CT and MRI show well-defined, usually bilateral, paraspinal masses, most commonly in the lower thoracic area. CT attenuation values and MRI signal intensity vary, according to the grade of hematologic activity of the lesion. Active lesions usually have soft-tissue density on CT and intermediate signal intensity on both T1- and T2-weighted MRI. Inactive lesions may have low or high attenuation values on CT, depending on the presence

of fat and iron content of the masses. For the same reason, inactive lesions have high signal intensity on both T1- and T2-weighted images if there is fatty replacement or low signal intensity with iron deposition. Mild homogeneous enhancement on both CT and MRI is usually seen in active lesions, whereas a heterogeneous enhancing pattern is more common in inactive lesions because of iron deposition or fatty replacement [48].

Intrathoracic Meningoceles: Spinal meningoceles are saccular protrusions of the meninges through intervertebral foramina or bone defects in one or more vertebrae. Meningoceles contain cerebrospinal fluid and usually occur in the thoracic spine, especially between T3 and T7 [50]. The protrusion can be anterior, lateral, anterolateral, or posterior to the vertebral body. Posterior meningoceles are the most common type, but they are not discussed in this review because they do not affect the posterior mediastinum. Most meningoceles are associated with syndromes, such as neurofibromatosis type 1. Small meningoceles are asymptomatic and can be discovered incidentally on a routine CXR, whereas larger lesions may compress the spinal cord, spinal nerves, and adjacent mediastinal structures. On CXR, meningoceles appear as paravertebral opacities with well-defined, smooth or lobulated borders. CT confirms a sharply defined, homogeneous, low-attenuation lesion up to 15 cm in diameter [50]. The lesion protrudes from the spinal canal into the posterior mediastinum and has a predominance for the right side, which might be related to the presence of the aorta on the left side. CT also reveals abnormalities in adjacent vertebrae and enlargement of intervertebral foramina. On MRI, meningoceles are cystic masses with the signal intensity of cerebrospinal fluid.

Mediastinal Abscesses: Mediastinal abscesses should be considered when a low-attenuation mass is identified at multidetector CT in a patient after surgery or esophageal perforation, or in the setting of infection in the adjacent thorax.

Pancreatic Pseudocysts: A cystic mass in the paravertebral mediastinum that develops over a short period of time in the clinical setting of pancreatitis may represent intrathoracic extension of a pancreatic pseudocyst [51]. These uncommon lesions contain pancreatic secretions, blood, and necrotic material and spread through the esophageal or aortic hiatus [52]. At multidetector CT, these lesions typically manifest as thin-walled masses that may be isoattenuating or hyperattenuating, depending on the presence of hemorrhage or infection. Separate intra-abdominal pseudocysts may or may not be present.

Conclusions

A wide variety of disorders can arise from the anatomical structures of the mediastinum. Each imaging modality plays a fundamental role in the detection and characterization of these disorders and in answering different morphologic questions to provide definite diagnostic information. The new mediastinal division scheme developed by ITMIG is designed to enable the precise identification of mediastinal abnormalities at cross-sectional imaging by radiologists and consistent

communication between healthcare providers. This system will improve lesion localization, help generate a focused differential diagnosis, and assist in tailoring biopsy and treatment plans.

References

1. Carter BW, Okumura M, Detterbeck FC, Marom EM. Approaching the patient with an anterior mediastinal mass: a guide for radiologists. J Thorac Oncol. 2014;9(9 Suppl 2):S110–8.
2. Carter BW, Marom EM, Detterbeck FC. Approaching the patient with an anterior mediastinal mass: a guide for clinicians. J Thorac Oncol. 2014;9(9 Suppl 2):S102–9.
3. Davis RD Jr, Oldham HN Jr, Sabiston DC Jr. Primary cysts and neoplasms of the mediastinum: recent changes in clinical presentation, methods of diagnosis, management, and results. Ann Thorac Surg. 1987;44:229–37.
4. Carter BW, Benveniste MF, Madan R, Godoy MC, de Groot PM, Truong MT, Rosado-de-Christenson ML, Marom EM. ITMIG classification of mediastinal compartments and multidisciplinary approach to mediastinal masses. Radiographics. 2017;37(2):413–36. Epub 2017 Jan 27.
5. Shields TW. Primary tumors and cysts of the mediastinum. In: Shields TW, editor. General thoracic surgery. Philadelphia: Lea & Febiger; 1983. p. 927–54.
6. Fraser RS, Müller NL, Colman N, Paré PD, editors. The mediastinum. In: Fraser and Paré's diagnosis of diseases of the chest. 4th ed. Philadelphia: Saunders; 1999. p. 196–234.
7. Fraser RG, Paré PA, editors. The normal chest. In: Diagnosis of diseases of the chest. 2nd ed. Philadelphia: Saunders; 1977. p. 1–183.
8. Felson B. Chest roentgenology. Philadelphia: Saunders; 1973.
9. Heitzman ER. The mediastinum. 2nd ed. New York: Springer; 1988.
10. Zylak CJ, Pallie W, Jackson R. Correlative anatomy and computed tomography: a module on the mediastinum. RadioGraphics. 1982;2(4):555–92.
11. Carter BW, Tomiyama N, Bhora FY, et al. A modern definition of mediastinal compartments. J Thorac Oncol. 2014;9(9 suppl 2):S97–S101.
12. Fujimoto K, Hara M, Tomiyama N, Kusumoto M, Sakai F, Fujii Y. Proposal for a new mediastinal compartment classification of transverse plane images according to the Japanese Association for Research on the Thymus (JART) General Rules for the Study of Mediastinal Tumors. Oncol Rep. 2014;31(2):565–72.
13. Rosado-de-Christenson ML, Templeton PA, Moran CA. Mediastinal germ cell tumors: radiologic and pathologic correlation. RadioGraphics. 1992;12(5):1013–30.
14. Ackman JB, Wu CC. MRI of the thymus. AJR Am J Roentgenol. 2011;197(1):W15–20.
15. Ackman JB. MR imaging of mediastinal masses. Magn Reson Imaging Clin N Am. 2015;23(2):141–64.
16. Carter BW, Benveniste MF, Truong MT, Marom EM. State of the art: MR imaging of thymoma. Magn Reson Imaging Clin N Am. 2015;23(2):165–77.
17. Sung YM, Lee KS, Kim BT, Choi JY, Shim YM, Yi CA. 18F-FDG PET/CT of thymic epithelial tumors: usefulness for distinguishing and staging tumor subgroups. J Nucl Med. 2006;47(10):1628–34.
18. Treglia G, Sadeghi R, Giovanella L, Cafarotti S, Filosso P, Lococo F. Is (18)F-FDG PET useful in predicting the WHO grade of malignancy in thymic epithelial tumors? A meta-analysis. Lung Cancer. 2014;86(1):5–13.
19. Jerushalmi J, Frenkel A, Bar-Shalom R, Khoury J, Israel O. Physiologic thymic uptake of 18F-FDG in children and young adults: a PET/CT evaluation of incidence, patterns, and relationship to treatment. J Nucl Med. 2009;50(6):849–53.

20. Detterbeck F. Clinical approach to mediastinal masses. In: Kuzdal JML, Muller M, Papagiannopoulos K, et al., editors. ESTS textbook of thoracic surgery. Exeter: European Society of Thoracic Surgeons; 2014.
21. Kim JH, Goo JM, Lee HJ, et al. Cystic tumors in the anterior mediastinum. Radiologic-pathological correlation. J Comput Assist Tomogr. 2003;27:714–23.
22. Merolla P, Falchetti A, Filosso P, et al. Thymic neuroendocrine carcinoma (carcinoid) in multiple endocrine neoplasia type 1 syndrome: the Italian series. J Clin Endocrinol Metab. 2005;90:2603–9.
23. Tomiyama N, Honda O, Tsubamoto M, et al. Anterior mediastinal tumors: diagnostic accuracy of CT and MRI. Eur J Radiol. 2009;69:280–8.
24. Inaoka T, Takahashi K, Mineta M, et al. Thymic hyperplasia and thymus gland tumors: differentiation with chemical shift MR imaging. Radiology. 2007;243:869–76.
25. Schaefer NG, Hany TF, Taverna C, et al. Non-Hodgkin lymphoma and Hodgkin disease: coregistered FDG PET and CT at staging and restaging—do we need contrast-enhanced CT? Radiology. 2004;232:823–9.
26. Naidich DP, Webb WR, Muller NL, Krinsky GA, Zerhouni EA, Siegelman SS, editors. Mediastinum. In: Computed tomography and magnetic resonance of the thorax. 3rd ed. Philadelphia: Lippincott Williams & Wilkins; 1999. p. 82–3.
27. Molinari F, Bankier AA, Eisenberg RL. Fat-containing lesions in adult thoracic imaging. AJR Am J Roentgenol. 2011;197(5):W795–813.
28. Nasseri F, Eftekhari F. Clinical and radiologic review of the normal and abnormal thymus: pearls and pitfalls. RadioGraphics. 2010;30(2):413–28.
29. Kissin CM, Husband JE, Nicholas D, Eversman W. Benign thymic enlargement in adults after chemotherapy: CT demonstration. Radiology. 1987;163(1):67–70.
30. Juanpere S, Cañete N, Ortuño P, Martínez S, Sanchez G, Bernado L. A diagnostic approach to the mediastinal masses. Insights Imaging. 2013;4(1):29–52.
31. Sirmali M, Turut H, Gezer S, et al. Clinical and radiologic evaluation of foramen of Morgagni hernias and the transthoracic approach. World J Surg. 2005;29:1520–4.
32. Rattan KN, Magu S, Rohilla S. Mediastinal foregut duplication cysts. Indian J Pediatr. 2004;71:103–5.
33. McAdams HP, Kirejczyk WM, Rosado-de-Christenson ML, Matsumoto S. Bronchogenic cyst: imaging features with clinical and histopathologic correlation. Radiology. 2000;217:441–6.
34. Botet JF, Lightdale C. Endoscopic sonography of the upper gastrointestinal tract. AJR Am J Roentgenol. 1991;156:63–8.
35. Felson B, Lessure AP. “Downhill” varices of the esophagus. Dis Chest. 1964;46:740–6.
36. Kim YJ, Raman SS, Yu NC, To’o KJ, Jutabha R, Lu DSK. Esophageal varices in cirrhotic patients: evaluation with liver CT. AJR Am J Roentgenol. 2007;188:139–44.
37. Lewis RB, Mehrotra AK, Rodriguez P, Levine MS. From the radiologic pathology archives: esophageal neoplasms: radiologic-pathologic correlation. Radiographics. 2013;33:1083–108.
38. Krasna MJ. Radiographic and endosonographic staging in esophageal cancer. Thorac Surg Clin. 2013;23:453–60.
39. van Rossum PS, van Hillegersberg R, Lever FM, et al. Imaging strategies in the management of oesophageal cancer: what’s the role of MRI? Eur Radiol. 2013;23:1753–65.
40. Kwee RM. Prediction of tumor response to neoadjuvant therapy in patients with esophageal cancer with use of 18F FDG PET: a systematic review. Radiology. 2010;254:707–17.
41. Hiratzka LF, Bakris GL, Beckman JA, et al. 2010 ACCF/AHA/AATS/ACR/ASA/SCA/SCAI/SIR/STS/SVM guidelines for the diagnosis and management of patients with thoracic aortic disease: a report of the American College of Cardiology Foundation/American Heart Association Task Force on Practice Guidelines, American Association for Thoracic Surgery, American College of Radiology, American Stroke Association, Society of Cardiovascular Anesthesiologists, Society for Cardiovascular Angiography and Interventions, Society of Interventional Radiology, Society of Thoracic Surgeons, and Society for Vascular Medicine. Circulation. 2010;121:e266–369.

42. Bickerstaff LK, Pairolero PC, Hollier LH, et al. Thoracic aortic aneurysms: a population-based study. Surgery. 1982;92:1103–8.
43. Upadhye S, Schiff K. Acute aortic dissection in the emergency department: diagnostic challenges and evidence-based management. Emerg Med Clin North Am. 2012;30:307–27.
44. Booher AM, Eagle KA. Diagnosis and management issues in thoracic aortic aneurysm. Am Heart J. 2011;162:38–46.
45. Bredella MA, Torriani M, Hornicek F, et al. Value of PET in the assessment of patients with neurofibromatosis type 1. AJR Am J Roentgenol. 2007;189(4):928–35.
46. Warbey VS, Ferner RE, Dunn JT, Calonje E, O'Doherty MJ. [18F]FDG PET/CT in the diagnosis of malignant peripheral nerve sheath tumours in neurofibromatosis type-1. Eur J Nucl Med Mol Imaging. 2009;36(5):751–7.
47. Restrepo CS, Eraso A, Ocazionez D, Lemos J, Martinez S, Lemos DF. The diaphragmatic crura and retrocrural space: normal imaging appearance, variants, and pathologic conditions. Radiographics. 2008;28:1289–305.
48. Baleriaux DL, Neugroschl C. Spinal and spinal cord infection. Eur Radiol. 2004;14(Suppl 3):E72–83.
49. Harisinghani MG, McLoud TC, Shepard JA, Ko JP, Shroff MM, Mueller PR. Tuberculosis from head to toe. Radiographics. 2000;20:449–70.
50. Miles J, Pennybacker J, Sheldon P. Intrathoracic meningocele: its development and association with neurofibromatosis. J Neurol Neurosurg Psychiatry. 1969;32(2):99–110.
51. Glazer HS, Siegel MJ, Sagel SS. Low-attenuation mediastinal masses on CT. AJR Am J Roentgenol. 1989;152(6):1173–7.
52. Kirchner SG, Heller RM, Smith CW. Pancreatic pseudocyst of the mediastinum. Radiology. 1977;123(1):37–42.